Clinical Integration of Quantitative Susceptibility Mapping Magnetic Resonance Imaging into Neurosurgical Practice

Sarah Kathleen Bandt, Ludovic de Rochefort, Weiwei Chen, Alexey Dimov, Pascal Spincemaille, Brian H. Kopell, Ajay Gupta, Yi Wang

Clinical Integration of Quantitative Susceptibility Mapping (QSM) MRI into Neurosurgical Practice

S. Kathleen Bandt, MD[1,2,3], Ludovic de Rochefort, PhD[1], Weiwei Chen, MD[4], Alexey V. Dimov, PhD[5], Pascal Spincemaille, PhD[6], Brian H. Kopell, MD[7], Ajay Gupta, MD[6], Yi Wang, PhD[1,5,6]

[1]Aix Marseille Université, CNRS, CRMBM UMR 7339, Marseille, France
[2]APHM, Hôpital de la Timone, CEMEREM, Marseille, France
[3]Northwestern University, Department of Neurological Surgery, Chicago, IL, USA
[4]Department of Radiology, Tongji Hospital, Wuhan, China
[5]Department of Biomedical Engineering, Cornell University, Ithaca, NY, USA
[6]Department of Radiology, Weill Cornell Medical College, New York, NY, USA
[7]Department of Neurosurgery, the Mount Sinai Hospital, New York, NY, USA

ACKNOWLEDGEMENT OF FUNDING SUPPORT: The authors would like to thank the American Association of Neurological Surgeons for their generous support via the William P. Van Wagenen Fellowship (SKB) which allowed this international collaboration to be possible.

DISCLOSURES: None for all authors

Corresponding Author:
S. Kathleen Bandt, MD
676 N. Saint Clair, Suite 2210
Chicago, IL 60611
Phone: (312) 695-0464
Email: skbandt@gmail.com

RUNNING TITLE: QSM in Neurosurgery

KEY WORDS: Quantitative Susceptibility Mapping, stereotactic navigation, advanced imaging techniques, deep brain stimulation, neuro-oncology, glioma, meningioma

ABBREVIATIONS: MRI: Magnetic Resonance Imaging; QSM: Quantitative Susceptibility Mapping; T1w: T1 weighted; T2w: T2 weighted; MRA: magnetic resonance angiography; SE: spine echo; GBM: Glioblastoma; DBS: deep brain stimulation; GRE: Gradient Echo; SWI: susceptibility weighted imaging; CM: cavernous malformation; BET: brain extraction; PD: Parkinson's Disease; GABA: gamma-Aminobutyric acid; STN: subthalamic nucleus; GPi: globus pallidus internus; PXA: pleomorphic xanthroastrocytoma; WHO: World Health Organization; FLAIR: fluid-attenuated inversion recovery

Abstract

Quantitative susceptibility mapping (QSM), a recently developed magnetic resonance imaging technique, is introduced to the field of neurosurgery. A brief overview of the physics behind the technique is provided for a neurosurgical audience. QSM is unique in its ability to offer a quantitative assessment of tissue magnetic susceptibility source, which has only been detected as a blooming artifact in gradient echo acquisition. Standard susceptibility weighted imaging cannot localize nor quantify susceptibility source. Clinical applications of QSM are wide-reaching and include precise localization of the deep nuclei for deep brain stimulation electrode placement, differentiation between blood products and calcification within brain lesions to optimize intra-operative preparedness during resection, and enhanced sensitivity of cerebral micrometastasis identification. QSM can be obtained in all patients able to undergo magnetic resonance imaging and is integratable into busy neuroradiology programs. Examples are provided for QSM's clinical applications in neurosurgical care. Clinical integration of QSM may help clinicians better identify and characterize neurosurgical lesions thereby improving patient care.

Introduction and Background

Magnetic resonance imaging (MRI) has revolutionized neurosurgery both for its use in diagnosis and surgical planning [1,2]. MRI generally provides three categories of biophysical information: 1) relaxation effects, providing information regarding the microenvironment for water proton interactions; 2) tissue transport processes, providing information regarding diffusion, perfusion and cerebral blood flow; and 3) molecular magnetism, providing information regarding tissue susceptibility and chemical shifts within cells. These categories may be interpreted as assessments of tissue cellularity, vascularity and biomolecularity respectively [3]. The first of these categories can be provided by spin echo (SE) and other sequences, including T1 weighted imaging (T1w) for defining gray and white matter anatomy and T2 weighted imaging (T2w) for characterizing pathological cellularity changes [2]. The second of these categories can be provided by sequences sensitive to tissue transport processes or vascularity, including contrast enhanced T1w (T1w+c) sequences probing the integrity of the blood brain barrier, diffusion and perfusion imaging, as well as magnetic resonance angiography (MRA) [2,3]. These first two categories represent the traditional work-horse MRI sequences that have fundamentally defined neurosurgical practice to date.

As the field of neurosurgery has evolved, particularly the expansion of functional neurosurgery [1,4], the shortcomings of these traditional brain MRI sequences have become evident. For example, increasing knowledge of brain circuits and their dysfunctions has facilitated the adaptation of deep brain stimulation (DBS) to treat a number of diseases and disorders [5-7]. Safe and effective placement of DBS electrodes requires the precise delineation of the deep nuclei for surgical targeting. However, traditional MRI is limited in its ability to visualize the deep nuclei [8], due to its poor sensitivity to the biomolecular composition of tissues [9]. Improving the ability to characterize the biomolecular properties of tissues is therefore desired -- which quantitative susceptibility mapping (QSM) [10] is capable of doing.

QSM is an imaging technique within the third category of MRI based on the gradient echo (GRE) sequence that is sensitive to the biomolecular magnetic properties of tissues, or tissue biomolecularity [3,11-14]. GRE has been used in various imaging methods, including T2* hypointense magnitude imaging (T2*w), a phase mask enhanced T2*w sequence known as susceptibility weighted imaging (SWI) [15,16], phase mapping [17,18], and QSM [10,11]. This third

category of MRI has been under-utilized overall due in large part to blooming artifact in which detection of susceptibility sources extend widely beyond their margins [19]. This blooming artifact results from a dipole field extending beyond its susceptibility source, making the source appear much larger radiographically than it is physically and distorting the source appearance in a manner dependent on its orientation in the scanner [19]. Furthermore, the phase image (a component of GRE imaging) has historically been discarded in conventional MRI protocols despite its routine acquisition. The GRE phase image contains information regarding the magnetic field experienced by water protons within tissue [17,20]. Blooming artifacts must still be contended with in phase imaging due to the fact that the magnetic field at any given location represents the sum of the contributions from all surrounding tissue susceptibilities. Together, these issues have resulted in this third category of MRI information having limited clinical applications to date [15,21]. By deconvolving the phase information to map tissue susceptibility sources [22], QSM opens the door to study tissue biomolecularity without blooming artifacts [9] and subsequently offers clinical neuroradiology and neurosurgery the opportunity to improve upon current shortcomings. QSM can be easily integrated into a busy clinical neuroradiology program requiring only a widely available gradient echo acquisition and an automated, off-line, processing pipeline which is free and readily available for installation. QSM results can be integrated into multiple neuronavigation platforms to aid both preoperative planning and intraoperative navigation.

As the magnetic moment of an electron is 658 times stronger than that of a proton [3], the electron clouds generate magnetic field over a much larger spatial range than the protons, and tissue biomolecularity is determined by molecular electron clouds. The fact that the magnetic field of the electron cloud is substantial on the macroscopic scale explains blooming artifacts in macroscopic GRE, both magnitude and phase imaging. Tissues with strongly paramagnetic susceptibility include the iron-storing tissues (such as the deep gray nuclei), veins containing deoxyheme, and hemorrhages with blood-degradation products. Tissue with strongly diamagnetic susceptibility includes calcification of concentrated hydroxyapatite crystal and white matter tracks of packed myelin.

In this report, we review the fundamentals of QSM, its workflow and integration, and we demonstrate a number of its distinct clinical applications into neurosurgical practice.

GRE Magnitude and Phase Imaging

GRE sequences are available on all MRI systems. GRE magnitude has T2* weighting (T2*w), which is a mixture of T2 weighting and intravoxel variation of the susceptibility field (R2'). Therefore, T2*w and SWI are more sensitive than T2w imaging for detecting tissue susceptibility [23]. SWI enhances susceptibility contrasts between different tissues [16,24]. SWI can be used for noninvasively imaging the venous system given its ability to detect paramagnetic deoxyhemoglobin in venous blood [25], identifying vascular malformations including arteriovenous malformations and cavernous malformations (CMs) [26,27], focal hemorrhage in the setting of brain tumors [28], and trauma [29]. SWI is advantageous in presurgical planning for epilepsy in the setting of a CM where resection not only of the CM itself but also the surrounding iron-stained tissue is required to maximize the chances of seizure freedom postoperatively [30]. Despite these applications of SWI into clinical neuroimaging, SWI has a major drawback of blooming artifacts that prevent it from precise mapping of the susceptibility sources necessary to guide neurosurgery. Another limitation of GRE magnitude-based imaging is the inability to differentiate between paramagnetic susceptibility sources (hemorrhage) and diamagnetic sources (calcification) [31] with each appearing radiographically similar.

GRE phase-based imaging has been explored to overcome SWI's inability to differentiate diamagnetic from paramagnetic sources [32]. Through phase filtering techniques [33], it is now possible to rapidly differentiate the sign of susceptibility sources on internal field maps: positive for paramagnetic iron, negative for diamagnetic calcification. While these advanced filtering approaches are superior compared to SWI and T2*w imaging [34], they are still not able to provide precise susceptibility source localization.

Quantitative Susceptibility Mapping (QSM)

QSM, as a postprocessing of GRE data without additional acquisition burden, enables quantification and localization of susceptibility sources seen as blooming artifacts on GRE magnitude and phase imaging. Prior to QSM, there had been a long history of attempts to quantify susceptibility artifact [9] but these were unsuccessful. The introduction of Bayesian inference with a morphological prior in 2008 set the groundwork for what would ultimately

become QSM [10,35]. Bayesian inference is a statistical method that estimates susceptibility from MR data and maps it back into radiographic image space. Using this approach, QSM accurately and precisely maps sources of susceptibility artifact in human tissue [9]. QSM has been shown to be reproducible across institutions as well as MR field strengths and scanner manufacturers, makes and models [9]. Furthermore, QSM processing can be performed off-line and is fully automated allowing for seamless clinical integration into a busy clinical neuroradiology program.

Brain QSM data can be easily acquired using a head-coil array and a 3D multi-echo GRE sequence on almost any MRI scanner, particularly on 3T systems optimized for the brain. Scan time varies between 5 and 10 minutes depending on desired spatial resolution. High-resolution (0.5mm isotropic) QSM of 10 min acquisition should be selected in the case of DBS targeting that requires anatomical precision. A routine brain QSM with high resolution in axial plane (0.6mm) of 5 min acquisition may suit for many imaging needs. While QSM recon remains an active area of research [36], most methods seem to converge to the use of a Bayesian cost function of data fidelity and structural consistency [10,37-43], and several recon software are available freely [44]. In a fully automated QSM recon implementation (email the senior author YW for installation details), upon completion of the acquisition, amplitude and phase DICOM images are sent to a separate, networked DICOM server (all major manufacturers allow proper phase image saving in their latest software versions). Reconstruction is automatically triggered for off-line QSM post-processing upon file arrival. When post-processing has been completed (approximately in 10 minutes), quantitative QSM, as well as magnitude (T2*w), phase, and SWI images (Figure 1) are ready for viewing. These may be sent on to radiology for review or neuronavigation stations for surgical planning.

Functional Neurosurgery Examples

Deep brain stimulation (DBS) has become a common treatment option for patients with Parkinson's disease (PD) [5,45], tremor [46], dystonia [7] and, increasingly, some psychiatric disorders [6]. Typically, DBS targets include the brain's deep gray nuclei. While the DBS mechanism of action is yet to be fully understood [47,48], efficacy of the treatment depends on precise targeting [49]. For example, successful DBS treatment of advanced PD requires implanting the active electrode contacts in the antero-lateral quadrant of the subthalamic nucleus (STN) with 0.5mm precision

[50]. Therefore, precise definition of the deep nuclei is critical for planning effective DBS placement.

Visualization of DBS targets has been challenging using traditional MRI sequences [51]. This may be explained by the lack of cellular contrast within the deep gray nuclei. Given the highly paramagnetic iron which is stored within neurons of the deep nuclei QSM can play an important role in defining the proper geometry of the deep nuclei through precise depiction of tissue iron content. For the STN, QSM has been shown to provide a superior contrast-to-noise ratio over other MRI methods, including T2w, T2*w, phase, and SWI [8]{Rasouli, 2018 #101}{Chandran, 2016 #103}. Below are some consented case examples demonstrating the clinical utility of QSM in functional neurosurgery practice.

Subthalamic nucleus (STN) localization

58 year old male with PD was offered bilateral STN DBS. QSM is performed pre-operatively for STN localization (Figure 2). Compared to T2w (Fig.1B), QSM (Fig.1C) provided markedly better spatial definition of STN geometry; QSM also illustrated iron decrease from the medial tip to the dorsolateral subdivision that was used as the DBS target.

Globus Pallidus internus (GPi) localization

11 year old male with generalized dystonia was offered DBS targeting the globus pallidus internus (GPi). QSM was performed pre-operatively for GPi localization (Figure 3). The medial medullary lamina depicted on QSM (Figure 3C) was useful in guiding DBS electrode placement.

Neurosurgical Oncology Examples

Traditional T1w and T2w SE imaging sensitive to cellularity has been very valuable for depicting brain tumor anatomy [2]. Yet, characterization of the heterogeneous cancer pathology on macroscopic imaging remains incomplete and is often inadequate for planning resection or radiotherapy [1,52]. Accompanying tumor cellularity changes include angiogenesis [53] and abnormal vasculature [54]. Angiogenesis in aggressive malignant tumors often causes hemorrhage, while apoptosis in benign tumors can lead to calcification. QSM is ideal for distinguishing between these tumoral tissue characteristics [31,55]{Tan, 2014 #108}{Ozbay, 2018 #109}. Below are some

consented case examples demonstrating the clinical utility of QSM in neurosurgical oncology practice.

Tumor characterization for surgical planning

Case 1. 54 year old female is found to have a heterogeneous, peri-ventricular mass in the left temporal lobe with surrounding edema on brain MRI. QSM identifies blood products within the solid portion of the tumor (Figure 4A and 4B). Patient is taken for resection of her solitary lesion which was resected en bloc due to the anticipated blood products. Pathology was consistent with metastatic renal cell carcinoma, a histologic diagnosis know to be associated with areas of hemorrhage.

Case 2. 48 year old female is found to have a large intra-ventricular lesion on brain MRI. QSM identifies dense calcification within the lesion (Figure 4C and 4D). Patient is taken for surgical resection where a firm, gritty mass is encountered. The lesion required aggressive ultrasonic aspiration in order to achieve gross total resection, as was anticipated based on preoperative QSM. Pathology was consistent with WHO grade I meningioma, a lesion which is known to frequently show dense regions of internal calcification.

Intraoperative navigation to maximize resection

58 year old male is found to have multiple intracranial lesions on brain MRI (Figure 5). Metastatic workup is unrevealing for evidence of a primary malignancy. Patient undergoes craniotomy for resection. Preoperative QSM was merged with neuronavigation enabling intraoperative localization of secondary and tertiary nodules facilitating gross total resection. Pathology was consistent with GBM.

Hemorrhagic micrometastasis identification

67 year old male with known non-small cell lung cancer is found to have new multi-focal metastatic disease on follow-up MRI. Three lesions are detected using standard imaging sequences. QSM identifies these three lesions but also identifies two additional lesions which were undetected using standard imaging sequences (Figure 6). The patient underwent radiosurgery for management of his intracranial disease.

Tumor histology correlation

Case 1. 15 year old male is found to have a heterogeneous mass within the right temporal lobe on MRI following a seizure. QSM does not demonstrate any susceptibility (Figure 7A and 7B) within the lesion. Pathology was consistent with WHO grade II pleomorphic xanthroastrocytoma, and as such, calcification or hemorrhage would not be expected in such a lesion As a result, the lack of signal abnormality on QSM would favor the diagnosis of a relatively less aggressive tumor such as a pleomorphic xantoastrocytoma. Higher grade neoplasms, on the other hand, such as a glioblastoma might be expected to show areas of internal hemorrhage and accordingly areas of increased susceptibility.

Case 2. 60 year old male is found to have a solitary lesion in the right frontal lobe extending across the corpus callosum on MRI. QSM demonstrates susceptibility consistent with internal blood products (Figure 7C and 7D). Patient was offered surgical debulking, pathology was consistent with WHO IV GBM.

Discussion

In this article, we have reviewed the basic principle of imaging tissue magnetic property. The GRE sequence can be used to sensitize the magnetic field induced by tissue magnetic susceptibility. The field can be extracted GRE phase data and deconvolved to reconstruct QSM for depicting and measuring susceptibility. QSM can be useful for neurological cases involving functional and pathological susceptibility contrasts. We have demonstrated clinically valuable examples of QSM applications in functional neurosurgery and in neurosurgical oncology.

Brain iron measured on QSM may be paramagnetic Fe3+ stored in ferritin, which is in biochemical equilibrium (homeostasis) with sparse Fe2+ that is bioactive but not measurable on QSM [9]. Iron is highly concentrated in deep gray nuclei that serve as hubs of brain circuits. These circuit activities require neurotransmitters, whose syntheses require iron as a catalyst [56]. The highly active brain circuits present rich iron for superb definition of deep gray nuclei on QSM. Furthermore, neurodegenerative diseases including Parkinson's disease are associated with dysfunctional iron homeostasis of iron overload at deep gray nuclei [57,58]. Therefore, deep gray nuclei as DBS targets can be excellently defined on QSM.

Brian tumor also involve pathological changes in tissue magnetic susceptibility. Rapid tumor growth involves leaking blood vessel formation with hemorrhage [59], which has paramagnetic Fe3+ stored in hemosiderin. Tumorous cells in certain types or parts of tumors may lack of blood supply, die, and decay into diamagnetic calcification [60]. QSM can be applied to measure and resolve hemorrhage and calcification for tumor characterization. This is particularly valuable for identifying surgical resection course of minimal bleeding.

Wide adaption of QSM in clinical practice requires easily-accessible fully-automated reconstruction. MRI manufacturers have to support proper saving of signal phase that traditionally has been largely discarded. Recent development of accurate and fast reconstruction using alternating direction method of multiplier may allow QSM implementation directly on scanner host computers with minimal programmable recon environments [43], such as Orchestra from General Electric Healthcare and ICE from Siemens Healthneer. These developments may facilitate QSM dissemination into clinics.

Conclusions

In summary, QSM is ideal for defining iron rich deep gray nuclei, and for characterizing and distinguishing between hemorrhage and tissue calcification. QSM can be integrated into busy neuroradiology programs due to its acceptable acquisition time and automated reconstruction workflow. Whenever an MRI protocol includes a GRE sequence, QSM should be post-processed without additional cost of scanner time. Clinical integration of QSM may help clinicians better identify and characterize neurosurgical targets thereby improving patient care.

Figure Captions:

Figure 1. GRE MRI of neurocysticercosis. A) magnitude (T2*w), B) phase (with high pass filtering), C) SWI, and D) QSM. T2*w, phase and SWI depict multiple lesions but cannot differentiate active hemorrhagic lesions from inactive calcified lesions. QSM demonstrates two hemorrhagic lesions with positive susceptibility (arrows) against calcified lesions with negative susceptibility.

Figure 2. STN localization using QSM. A) diagrammatic representation of deep nuclei anatomy in coronal section at the level of the STN; B) coronal cross-section through T2w image; C) coronal cross-section through post-processed QSM image highlighting visualization of the STN.

Figure 3. GPi localization using QSM. A) diagrammatic representation of deep nuclei anatomy in coronal section at the level of the GPi; B) coronal and C) axial cross-sections through post-processed QSM image highlighting visualization of the globus pallidus.

Figure 4. Tumor characterization using QSM. Hemorrhagic in renal cell carcinoma metastasis on A) T2w and B) QSM images, compared to partially calcified meningioma on C) T2w and D) QSM images. Note the hyperintense signal on QSM images in the hemorrhagic mass in panel B, compared to the predominantly hypointense signal on QSM images in the partially calcified mass in panel D.

F**igure 5. Multi-focal glioblastoma.** Axial representation of multi-focal glioblastoma on A) T1w B) T2w, C) FLAIR, and D) QSM images. Note areas of hemorrhage clearly depicted as regions of hyperintensity on QSM images in panel D.

Figure 6. Multi-focal mestastatic disease. QSM improves the conspicuity of multi-focal micrometastatic disease. Panels A) and D) demonstrate subtle findings on T1w+c images, similarly subtle findings on FLAIR imaging shown in panels B) and E) while more noticeable

abnormalities are visualized on post-processed QSM images shown in panels C) and F). Arrows identify location of lesions as seen on QSM.

Figure 7. Tumor histology anticipation to guide surgical strategy. Axial slices demonstrating A) WHO Grade II pleomorphic xanthroastrocytoma (PXA) on T1w+c imaging and B) without evidence of either hemorrhage or calcification on QSM. Findings are contrasted against those in WHO Grade IV GBM. Panel C) GBM on T1w+c imaging and D) QSM. Note that QSM reveals no significant abnormal findings in the Grade II PXA while it demonstrates a thick, irregular rim of increased susceptibility peripherally with foci of internal increased susceptibility within the grade IV GBM.

References

1. Golby AJ. *Image-Guided Neurosurgery.* Elsevier Science; 2015.
2. Atlas SW. *Magnetic Resonance Imaging of the Brain and Spine.* Lippincott Williams & Wilkins; 2016.
3. Wang Y. *Principles of Magnetic Resonance Imaging: Physics Concepts, Pulse Sequences, & Biomedical Applications.* CreateSpace Independent Publishing Platform; 2012.
4. Lumenta CB. *Neurosurgery.* Heidelberg: Springer; 2010.
5. Benabid AL. Deep brain stimulation for Parkinson's disease. *Curr Opin Neurobiol.* 2003;13(6):696-706.
6. Graat I, Figee M, Denys D. The application of deep brain stimulation in the treatment of psychiatric disorders. *Int Rev Psychiatry.* 2017;29(2):178-190.
7. Vercueil L, Pollak P, Fraix V, et al. Deep brain stimulation in the treatment of severe dystonia. *J Neurol.* 2001;248(8):695-700.
8. Liu T, Eskreis-Winkler S, Schweitzer AD, et al. Improved subthalamic nucleus depiction with quantitative susceptibility mapping. *Radiology.* 2013;269(1):216-223.
9. Wang Y, Spincemaille P, Liu Z, et al. Clinical quantitative susceptibility mapping (QSM): Biometal imaging and its emerging roles in patient care. *J Magn Reson Imaging.* 2017.
10. de Rochefort L, Liu T, Kressler B, et al. Quantitative susceptibility map reconstruction from MR phase data using bayesian regularization: validation and application to brain imaging. *Magn Reson Med.* 2010;63(1):194-206.
11. Wang Y, Liu T. Quantitative susceptibility mapping (QSM): Decoding MRI data for a tissue magnetic biomarker. *Magn Reson Med.* 2015;73(1):82-101.
12. Haacke EM, Liu S, Buch S, Zheng W, Wu D, Ye Y. Quantitative susceptibility mapping: current status and future directions. *Magnetic resonance imaging.* 2015;33(1):1-25.
13. Deistung A, Schweser F, Reichenbach JR. Overview of quantitative susceptibility mapping. *NMR Biomed.* 2016.
14. Liu C, Wei H, Gong NJ, Cronin M, Dibb R, Decker K. Quantitative Susceptibility Mapping: Contrast Mechanisms and Clinical Applications. *Tomography.* 2015;1(1):3-17.
15. Haacke EM, Reichenbach J. *Susceptibility Weighted Imaging in MRI: Basic Concepts and Clinical Applications.* New York: Wiley-Blackwell; 2011.
16. Haacke EM, Xu Y, Cheng YC, Reichenbach JR. Susceptibility weighted imaging (SWI). *Magn Reson Med.* 2004;52(3):612-618.
17. Schweser F, Deistung A, Reichenbach JR. Foundations of MRI phase imaging and processing for Quantitative Susceptibility Mapping (QSM). *Z Med Phys.* 2016;26(1):6-34.
18. Wharton S, Bowtell R. Fiber orientation-dependent white matter contrast in gradient echo MRI. *Proceedings of the National Academy of Sciences of the United States of America.* 2012;109(45):18559-18564.
19. Li J, Chang S, Liu T, et al. Reducing the object orientation dependence of susceptibility effects in gradient echo MRI through quantitative susceptibility mapping. *Magn Reson Med.* 2012;68(5):1563-1569.
20. Ghiglia DC, Pritt MD. *Two-dimensional phase unwrapping : theory, algorithms, and software.* New York: Wiley; 1998.

21. Mittal S, Wu Z, Neelavalli J, Haacke EM. Susceptibility-weighted imaging: technical aspects and clinical applications, part 2. *AJNR Am J Neuroradiol.* 2009;30(2):232-252.
22. Wang Y. *Quantitative Susceptibility Mapping: Magnetic Resonance Imaging of Tissue Magnetism.* Createspace Independent Pub; 2013.
23. Ito K, Mitchell DG, Gabata T, et al. Hepatocellular carcinoma: association with increased iron deposition in the cirrhotic liver at MR imaging. *Radiology.* 1999;212(1):235-240.
24. de Crespigny AJ, Roberts TP, Kucharcyzk J, Moseley ME. Improved sensitivity to magnetic susceptibility contrast. *Magn Reson Med.* 1993;30(1):135-137.
25. Reichenbach JR, Essig M, Haacke EM, et al. High-resolution venography of the brain using magnetic resonance imaging. *MAGMA.* 1998;6(1):62-69.
26. Essig M, Reichenbach JR, Schad L, Debus J, Kaiser WA. [High resolution MR-venography of cerebral arteriovenous malformations]. *Radiologe.* 2001;41(3):288-295.
27. de Souza JM, Domingues RC, Cruz LC, Jr., Domingues FS, Iasbeck T, Gasparetto EL. Susceptibility-weighted imaging for the evaluation of patients with familial cerebral cavernous malformations: a comparison with t2-weighted fast spin-echo and gradient-echo sequences. *AJNR Am J Neuroradiol.* 2008;29(1):154-158.
28. Sehgal V, Delproposto Z, Haddar D, et al. Susceptibility-weighted imaging to visualize blood products and improve tumor contrast in the study of brain masses. *J Magn Reson Imaging.* 2006;24(1):41-51.
29. Park JH, Park SW, Kang SH, Nam TK, Min BK, Hwang SN. Detection of traumatic cerebral microbleeds by susceptibility-weighted image of MRI. *J Korean Neurosurg Soc.* 2009;46(4):365-369.
30. Baumann CR, Schuknecht B, Lo Russo G, et al. Seizure outcome after resection of cavernous malformations is better when surrounding hemosiderin-stained brain also is removed. *Epilepsia.* 2006;47(3):563-566.
31. Chen W, Zhu W, Kovanlikaya I, et al. Intracranial calcifications and hemorrhages: characterization with quantitative susceptibility mapping. *Radiology.* 2014;270(2):496-505.
32. Deistung A, Mentzel H-J, Rauscher A, Witoszynskyj S, Kaiser WA, Reichenbach JR. Demonstration of paramagnetic and diamagnetic cerebral lesions by using susceptibility weighted phase imaging (SWI). *Zeitschrift für Medizinische Physik.* 2006;16(4):261-267.
33. Kaaouana T, de Rochefort L, Samaille T, et al. 2D harmonic filtering of MR phase images in multicenter clinical setting: toward a magnetic signature of cerebral microbleeds. *Neuroimage.* 2015;104:287-300.
34. Kaaouana T, Bertrand A, Ouamer F, et al. Improved cerebral microbleeds detection using their magnetic signature on T2*-phase-contrast: A comparison study in a clinical setting. *Neuroimage Clin.* 2017;15:274-283.
35. de Rochefort L, Brown R, Prince MR, Wang Y. Quantitative MR susceptibility mapping using piece-wise constant regularized inversion of the magnetic field. *Magn Reson Med.* 2008;60(4):1003-1009.
36. Langkammer C, Schweser F, Shmueli K, et al. Quantitative susceptibility mapping: Report from the 2016 reconstruction challenge. *Magn Reson Med.* 2018;79(3):1661-1673.
37. Liu J, Liu T, de Rochefort L, et al. Morphology enabled dipole inversion for quantitative susceptibility mapping using structural consistency between the magnitude image and the susceptibility map. *NeuroImage.* 2012;59(3):2560-2568.

38. Schweser F, Sommer K, Deistung A, Reichenbach JR. Quantitative susceptibility mapping for investigating subtle susceptibility variations in the human brain. *NeuroImage.* 2012;62(3):2083-2100.
39. Li W, Wang N, Yu F, et al. A method for estimating and removing streaking artifacts in quantitative susceptibility mapping. *NeuroImage.* 2015;108:111-122.
40. Langkammer C, Bredies K, Poser BA, et al. Fast quantitative susceptibility mapping using 3D EPI and total generalized variation. *Neuroimage.* 2015;111:622-630.
41. Bao L, Li X, Cai C, Chen Z, van Zijl PC. Quantitative Susceptibility Mapping Using Structural Feature Based Collaborative Reconstruction (SFCR) in the Human Brain. *IEEE Trans Med Imaging.* 2016;35(9):2040-2050.
42. Sun H, Kate M, Gioia LC, Emery DJ, Butcher K, Wilman AH. Quantitative susceptibility mapping using a superposed dipole inversion method: Application to intracranial hemorrhage. *Magn Reson Med.* 2016;76(3):781-791.
43. Milovic C, Bilgic B, Zhao B, Acosta-Cabronero J, Tejos C. Fast nonlinear susceptibility inversion with variational regularization. *Magn Reson Med.* 2018;80(2):814-821.
44. QSM. MEDI: http://weill.cornell.edu/mri/pages/qsm.html; STI.Suite, https://people.eecs.berkeley.edu/~chunlei.liu/software.html; ADMM: https://martinos.org/~berkin/publications.html; SWIM: http://www.swim-mri.com/index.php?site=software; TGV: http://www.neuroimaging.at/pages/qsm.php. 2018.
45. Weaver FM, Follett K, Stern M, et al. Bilateral deep brain stimulation vs best medical therapy for patients with advanced Parkinson disease: a randomized controlled trial. *JAMA.* 2009;301(1):63-73.
46. Rehncrona S, Johnels B, Widner H, Tornqvist AL, Hariz M, Sydow O. Long-term efficacy of thalamic deep brain stimulation for tremor: double-blind assessments. *Mov Disord.* 2003;18(2):163-170.
47. Brown P, Williams D. Basal ganglia local field potential activity: character and functional significance in the human. *Clin Neurophysiol.* 2005;116(11):2510-2519.
48. Wichmann T, Delong MR. Deep brain stimulation for neurologic and neuropsychiatric disorders. *Neuron.* 2006;52(1):197-204.
49. Benabid AL, Chabardes S, Mitrofanis J, Pollak P. Deep brain stimulation of the subthalamic nucleus for the treatment of Parkinson's disease. *Lancet Neurol.* 2009;8(1):67-81.
50. Wodarg F, Herzog J, Reese R, et al. Stimulation site within the MRI-defined STN predicts postoperative motor outcome. *Movement disorders : official journal of the Movement Disorder Society.* 2012;27(7):874-879.
51. Cho ZH, Min HK, Oh SH, et al. Direct visualization of deep brain stimulation targets in Parkinson disease with the use of 7-tesla magnetic resonance imaging. *J Neurosurg.* 2010;113(3):639-647.
52. Jain R, Essig M. *Brain Tumor Imaging.* Thieme; 2015.
53. Jain RK, di Tomaso E, Duda DG, Loeffler JS, Sorensen AG, Batchelor TT. Angiogenesis in brain tumours. *Nat Rev Neurosci.* 2007;8(8):610-622.
54. Nagy JA, Chang SH, Dvorak AM, Dvorak HF. Why are tumour blood vessels abnormal and why is it important to know? *Br J Cancer.* 2009;100(6):865-869.

55. Deistung A, Schweser F, Wiestler B, et al. Quantitative susceptibility mapping differentiates between blood depositions and calcifications in patients with glioblastoma. *PLoS One.* 2013;8(3):e57924.
56. Aisen P, Enns C, Wessling-Resnick M. Chemistry and biology of eukaryotic iron metabolism. *Int J Biochem Cell Biol.* 2001;33(10):940-959.
57. Zecca L, Youdim MB, Riederer P, Connor JR, Crichton RR. Iron, brain ageing and neurodegenerative disorders. *Nature reviews Neuroscience.* 2004;5(11):863-873.
58. Du G, Liu T, Lewis MM, et al. Quantitative susceptibility mapping of the midbrain in Parkinson's disease. *Movement disorders : official journal of the Movement Disorder Society.* 2016;31(3):317-324.
59. McDonald DM, Baluk P. Significance of blood vessel leakiness in cancer. *Cancer Res.* 2002;62(18):5381-5385.
60. Kim KM. Apoptosis and calcification. *Scanning Microsc.* 1995;9(4):1137-1175; discussion 1175-1138.

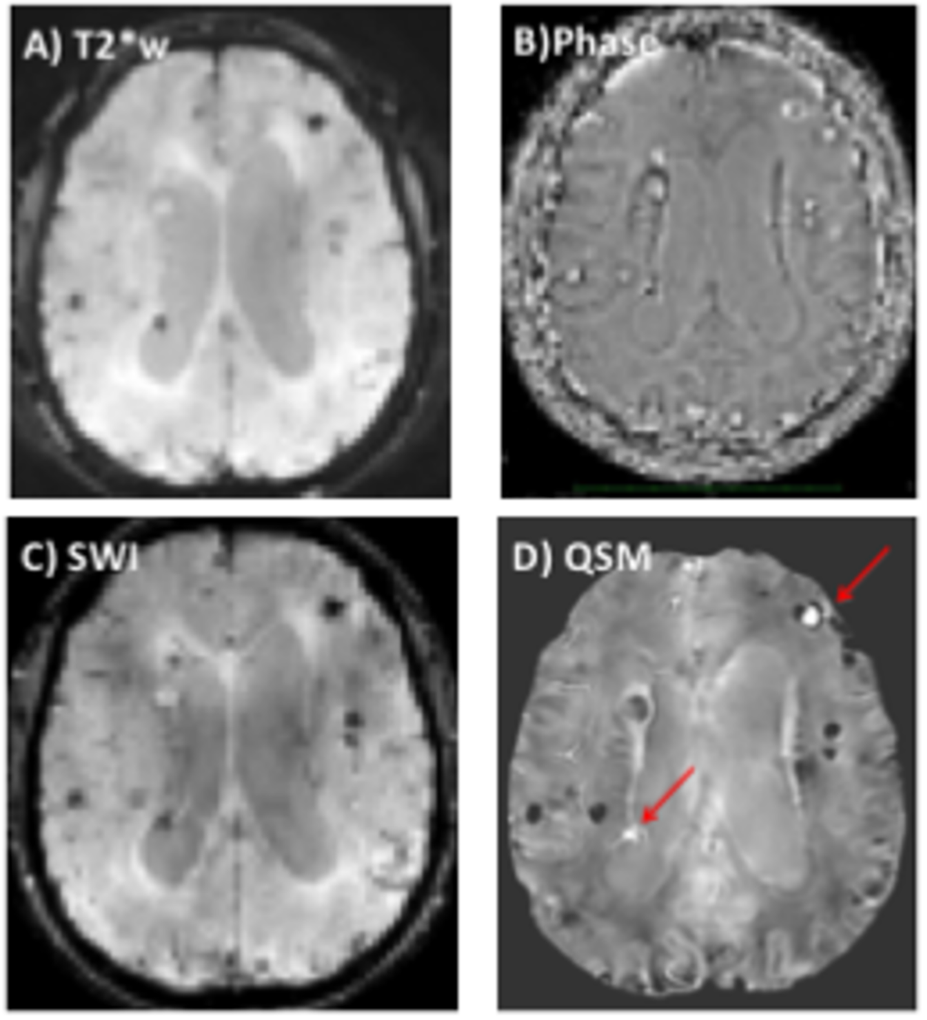
A) T2*w
B)Phase
C) SWI
D) QSM

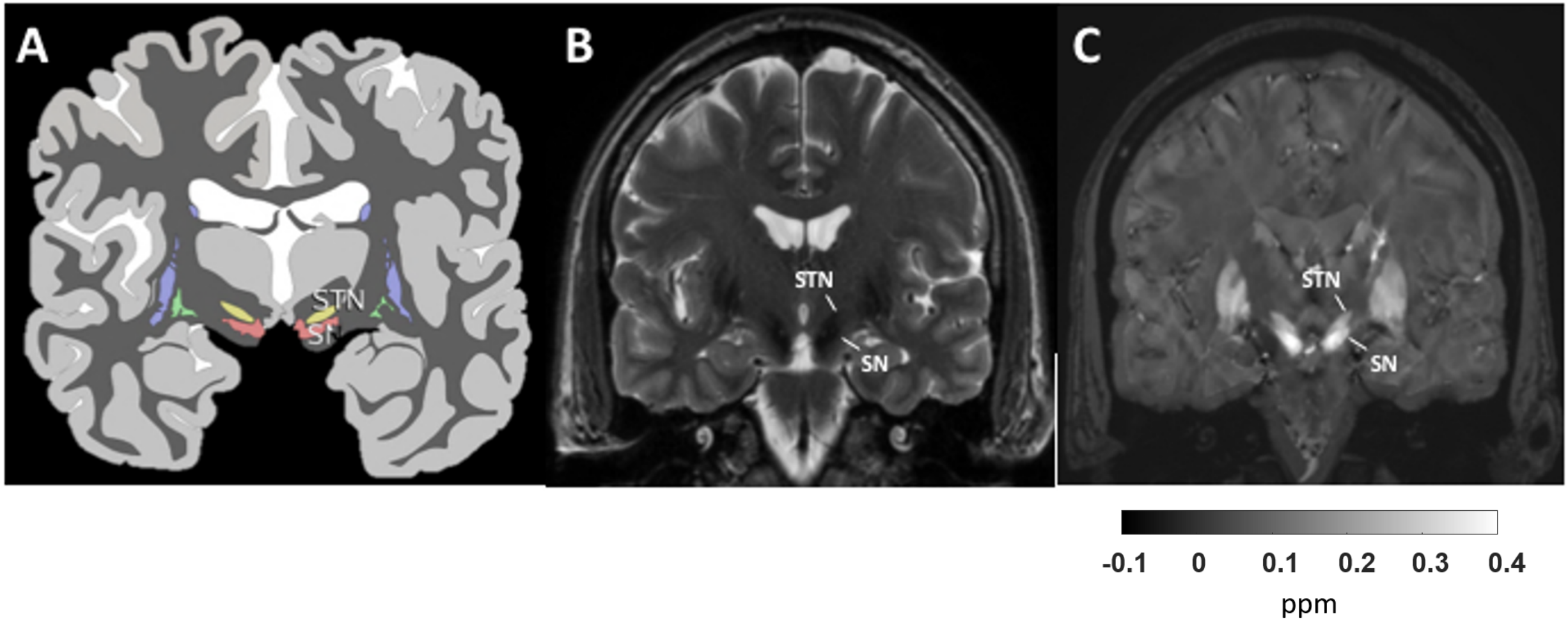
A
STN
SN
B
STN
SN
C
STN
SN
-0.1
0
0.1
0.2
0.3
0.4
ppm

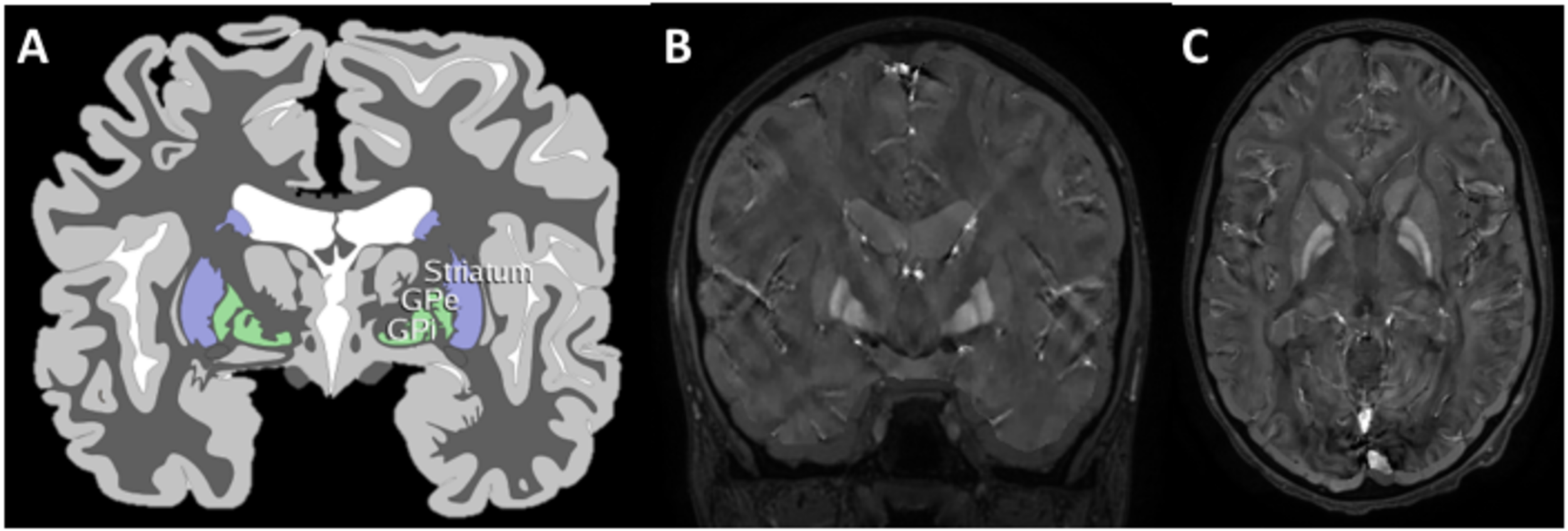
A
Striatum
GPe
GPi
B
C

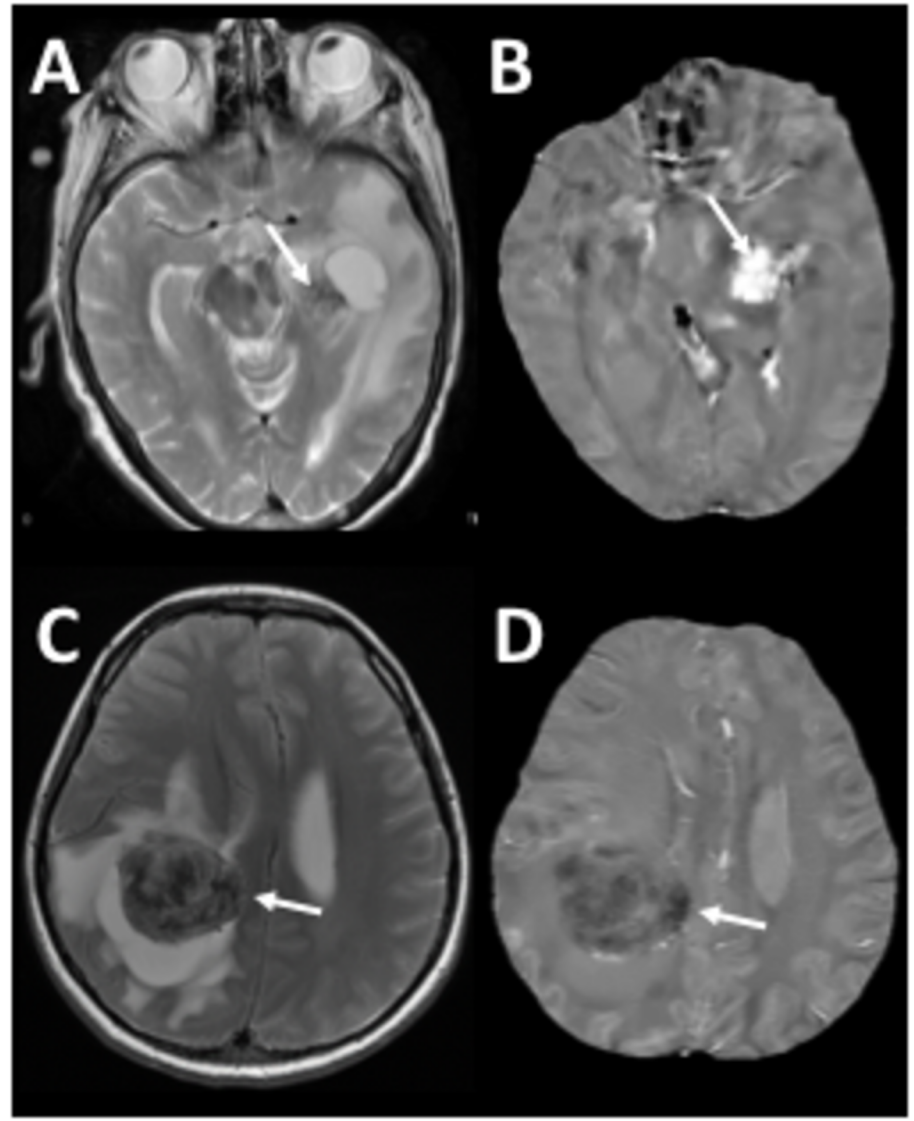
A
B
C
D

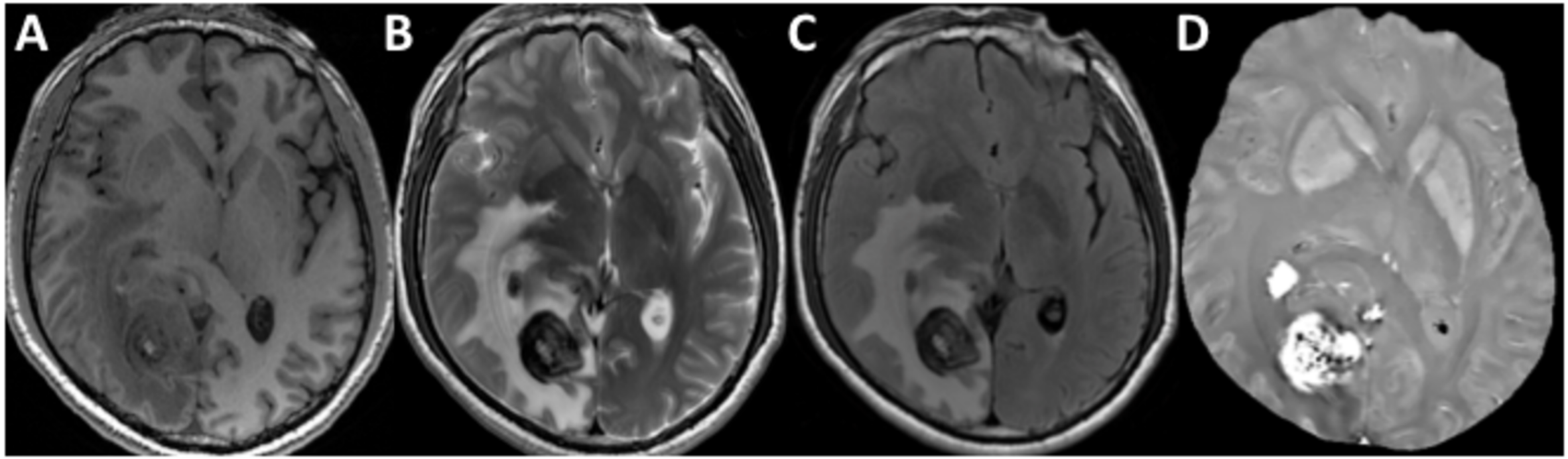
A
B
C
D

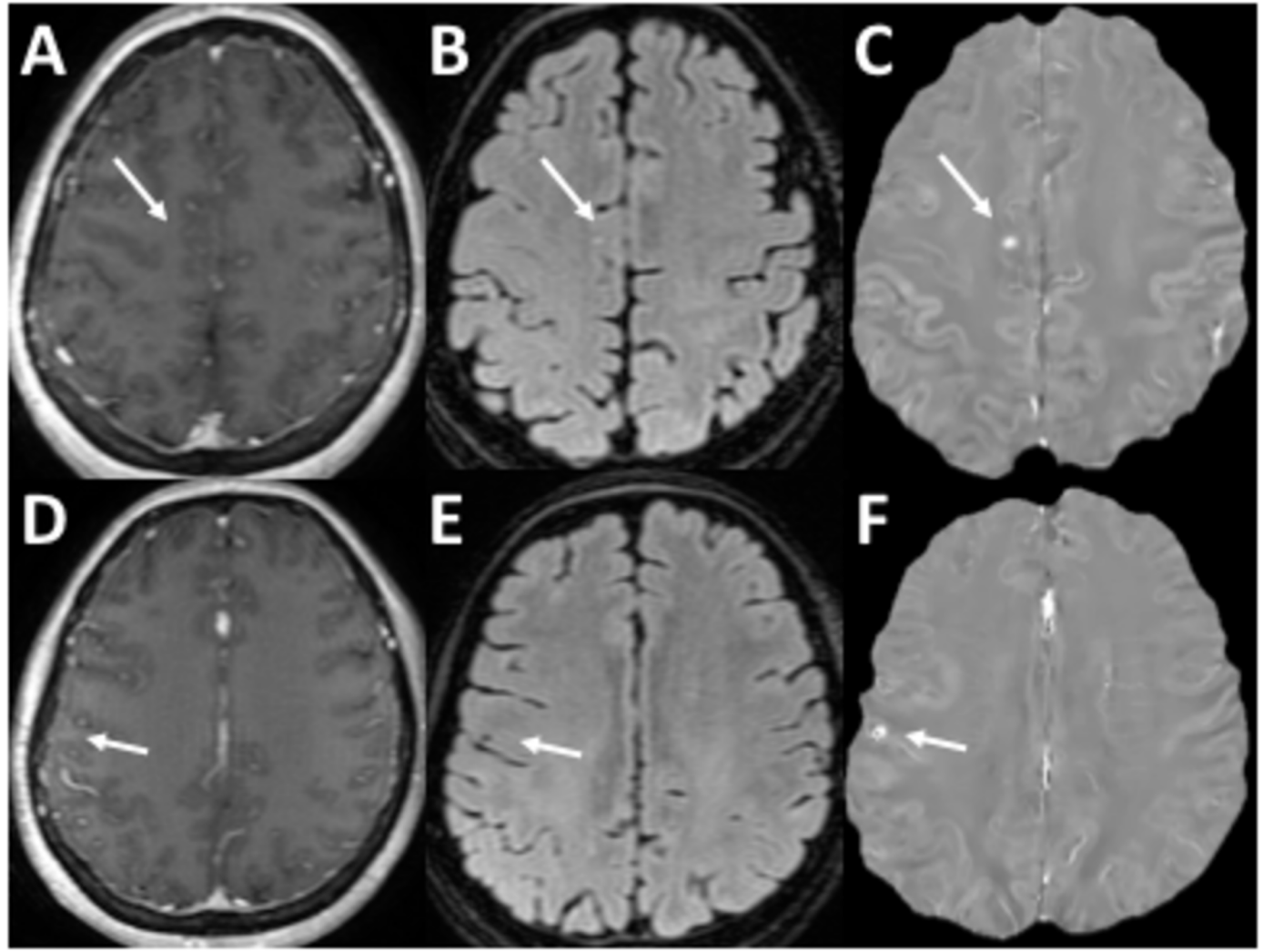
A
B
C
D
E
F

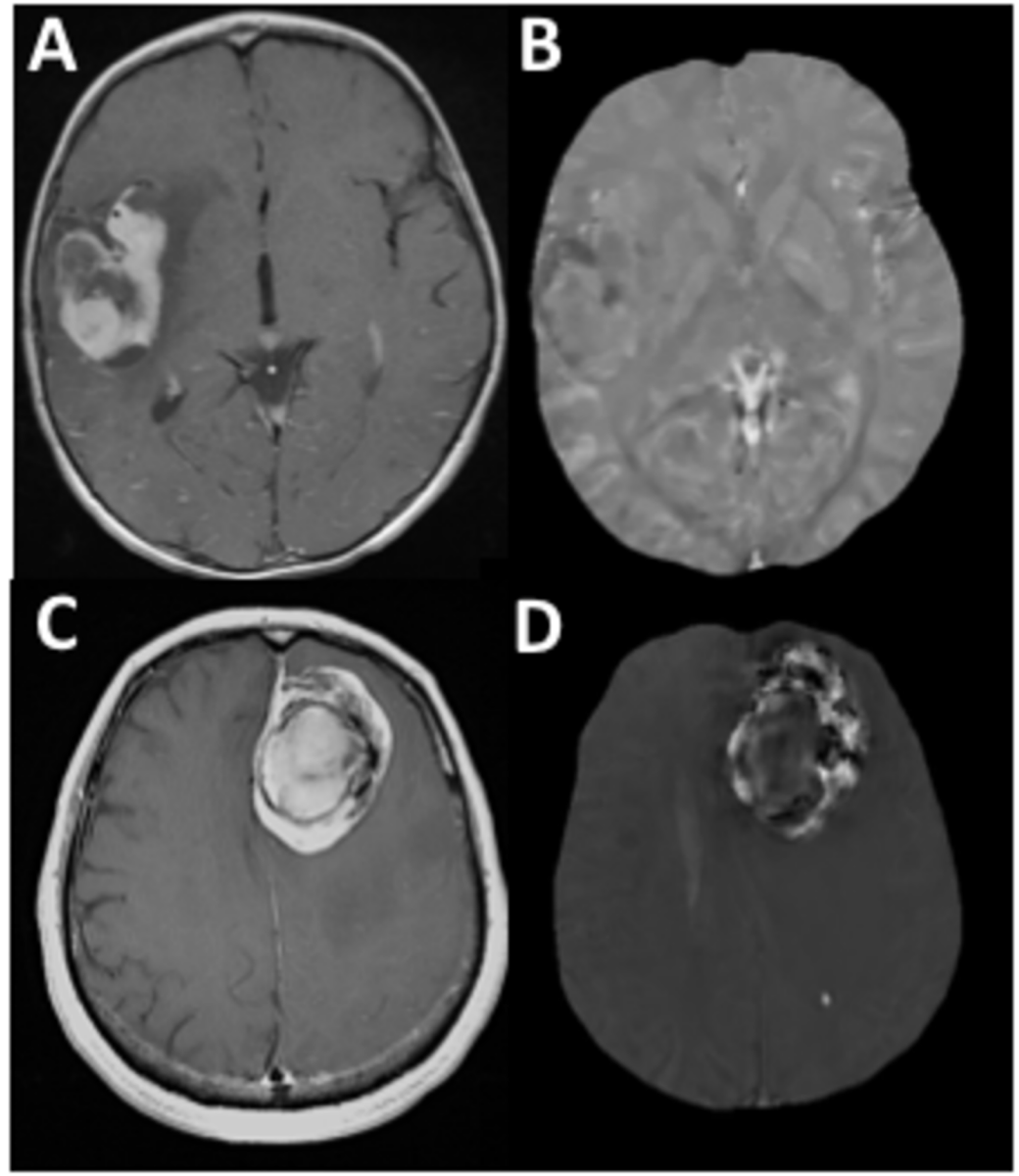
A
B
C
D